Autonomous Navigation of a Robotic Swarm in Space Exploration Missions

Siwei Zhang, Tobias Baumgartner, Emanuel Staudinger,
Robert Pöhlmann, Fabio Broghammer and Armin Dammann

Institute of Communications and Navigation, German Aerospace Center (DLR), Germany
Email: Siwei.Zhang@dlr.de

***Abstract*—In recent years, the paradigm of navigation has shifted from pinpointing the location of a single agent to continuously estimating the full kinematic state of networked autonomous agents. In this paper, we propose a kinematics-aware information seeking algorithm for swarm navigation. The algorithm tightly couples state estimation and autonomous control given ranging and kinematic models. With the help of the Fisher information theory, agents generate information seeking command sequences. As an outcome, the swarm continuously optimizes its trajectory so that the agents' position and orientation uncertainty is actively minimized. The proposed algorithm is verified by large-scale swarm simulations and demonstrated in a space-analogue mission of autonomous swarm navigation on the volcano Mount Etna.**

I. Introduction

The European Union envisions swarm robotics as one of the top innovation breakthroughs by 2038 [1]. A robotic swarm is an autonomous multi-robot system that is capable of solving complex tasks, e.g. sensing and exploration, of large areas that are difficult to access [2]–[4]. A robot in a swarm is also known as an *agent*. The collection of positions of all agents is called a *formation*. Compared with a single robot, a swarm is especially attractive for extraterrestrial surface exploration. As an example, a conceptual lunar swarm exploration mission [5] is depicted in Figure 1. A swarm of robots (in green) depart from the landing site, scout the area of interest, and deploy a low frequency array (in blue) to observe radio bursts from Jupiter. To achieve these tasks autonomously, the agents need to be aware of their positions and orientations. Without a global navigation satellite system, a swarm on extraterrestrial missions can exploit the radio signals that are exchanged in the network to localize itself via multilateration. Anchors for example a lander and two sensor boxes with known positions at the landing site (marked in red in Figure 1) provide a navigational coordinate system for swarm localization. The accuracy of multilateration depends on the observation models and the formation, which is quantified by Fisher information (FI). Finding and maintaining preferable formations for localization while exploring can be posed as a prerequisite task to the main mission. In [6], [7], abstract methods dubbed *position information seeking (PIS)* have been proposed, where agents are considered as mass points that "jump" from location to location to approach optimized formations maximizing FI. In real-world, preferred formations are often defined in the navigational coordinate system. However, the actuator of a robot can only execute control commands, like linear and angular velocities, with respect to (w.r.t.) its body coordinate system. Therefore, the agents need to possess precise knowledge of their positions, orientations and kinematic models to generate effective navigation strategies.

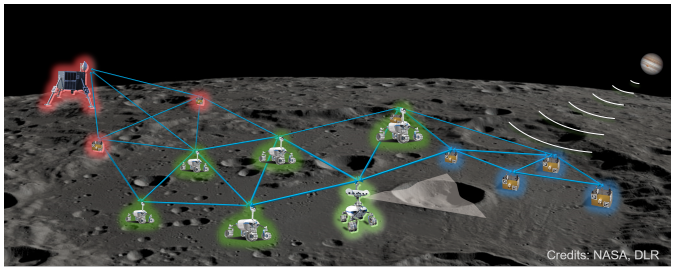

Figure 1: Conceptual lunar swarm mission for geological exploration and radio astronomy.

In this paper, we introduce a *kinematics-aware information seeking (KIS)* method, extending the PIS framework in [7]. The posterior Cramér-Rao lower bound (PCRLB) is exploited to formulate the formation optimization problem in KIS. The agents plan smooth trajectories accounting for their kinematic models. As an outcome, the swarm's formation is actively optimized, so that the agents' position and orientation information jointly increase. We analyze the mathematical expression of the PCRLB, and draw intuitive interpretation on the expected swarm behaviors emerging from KIS. The proposed KIS method is verified with a large-scale swarm simulation and demonstrated in a space-analogue mission on the volcano Etna, Sicily, Italy, in July 2022. The emerging swarm behaviors from both simulation and experiment coincide with the theoretical analysis, which verifies the effectiveness of the proposed KIS method.

II. Problem Formulation

A. Kinematic models

In [8], a 15 dimensional state space has been designed for distributed particle filtering (DPF) for swarm navigation in 3D.

In this paper, we focus on the kinematics of ground rovers operating in a 2D plane. We consider a swarm composed of N agents with their positions $\boldsymbol{p}_i = \begin{bmatrix} x_i, y_i \end{bmatrix}^{\mathrm{T}}$ and their headings ϕ_i defined as the angles from the positive x-axis to the pointing directions of the rovers, where $i = 1, \dots, N$. The state of the swarm is obtained by stacking all positions and headings

$$\boldsymbol{x} = \begin{bmatrix} \boldsymbol{p}^{\mathrm{T}}, \boldsymbol{\phi}^{\mathrm{T}} \end{bmatrix}^{\mathrm{T}} = \begin{bmatrix} \boldsymbol{p}_1^{\mathrm{T}}, \cdots, \boldsymbol{p}_N^{\mathrm{T}}, \phi_1, \cdots, \phi_N \end{bmatrix}^{\mathrm{T}} \in \mathbb{R}^{3N}. \quad (1)$$

The i^{th} rover is controlled by its velocity v_i and turning rate ω_i commands. By stacking the controls of all rovers, we obtain the control vector

$$\boldsymbol{u} = \begin{bmatrix} \boldsymbol{v}^{\mathrm{T}}, \boldsymbol{\omega}^{\mathrm{T}} \end{bmatrix}^{\mathrm{T}} = \begin{bmatrix} v_1, \cdots, v_N, \omega_1 \cdots, \omega_N \end{bmatrix}^{\mathrm{T}} \in \mathbb{R}^{2N}. \quad (2)$$

The state transition of a rover i is described by the coordinated turn model [9, p. 206]:

$$\begin{bmatrix} x_i^+ \\ y_i^+ \\ \phi_i^+ \end{bmatrix} = \begin{bmatrix} x_i \\ y_i \\ \phi_i \end{bmatrix} + T \begin{bmatrix} v_i \left(\mathrm{si}(\omega_i T) \cos(\phi_i) + \mathrm{co}(\omega_i T) \sin(\phi_i) \right) \\ v_i \left(\mathrm{si}(\omega_i T) \sin(\phi_i) - \mathrm{co}(\omega_i T) \cos(\phi_i) \right) \\ \omega_i \end{bmatrix} \quad (3)$$

where $\mathrm{si}(x) = \frac{\sin(x)}{x}$ and $\mathrm{co}(x) = \frac{\cos(x)-1}{x}$ and T is the time of executing constant velocity v_i and turning rate ω_i. We use notation $(\cdot)^+$ to denote state advancement over T. The state transition of the whole swarm can be expressed as a function of the current state and the controls, i.e.

$$\boldsymbol{x}^+ = f(\boldsymbol{x}, \boldsymbol{u}). \quad (4)$$

The term $\boldsymbol{u}$ denotes the exact controls that the actuators execute. The measured controls, for example from an inertial measurement unit (IMU), odometry, or command inputs, are denoted as $\hat{\boldsymbol{u}} = [\hat{\boldsymbol{v}}^{\mathrm{T}}, \hat{\boldsymbol{\omega}}^{\mathrm{T}}]^{\mathrm{T}}$, which are distorted by independent additive white Gaussian noise (AWGN), with a diagonal covariance matrix $\mathbb{\Sigma}_{\hat{\boldsymbol{u}}} = \mathrm{diag}\{\mathbb{\Sigma}_{\hat{\boldsymbol{v}}}, \mathbb{\Sigma}_{\hat{\boldsymbol{\omega}}}\}$.

We assume a maximum admissible velocity $v_{\max}$, turning rate $\omega_{\max}$, and a minimal turning radius $r_{\min}$, which define the set of admissible commands

$$\mathcal{V} = \left\{ \boldsymbol{u} \;\middle|\; {}_{|v_i| \le v_{\max}, |\omega_i| \le \omega_{\max}, |\omega_i| r_{\min} \le |v_i|, \forall\ 1 \le i \le N} \right\}. \quad (5)$$

The state space, transition model and admissible control space collectively define the kinematics of a rover, which are visualized in Figure 2.

B. Ranging measurements

We consider that agents obtain ranging measurements by exchanging radio frequency (RF) signals and measuring round trip time (RTT). We further assume the clock imperfection has been pre-compensated [11]. The ranging measurement $\hat{d}_{ij}$ between two nodes i and j is modeled as

$$\hat{d}_{ij} = d_{ij} + \epsilon_{ij}, \quad (6)$$

with the true distance d_{ij} distorted by AWGN ϵ_{ij} with distance-dependent variance $\sigma_{ij}^2(d_{ij})$. The variance is modeled as in [7], which is quadratically proportional to the distance, until reaching the maximum communication distance.

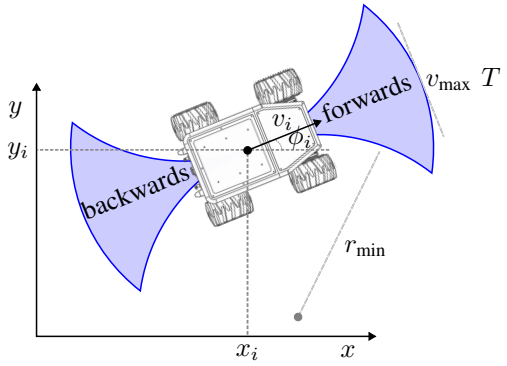

Figure 2: Kinematics of rover i is defined by the state space, transition model and admissible control space. An image of a summit-XL rover [10], which is used as a robotic platform for swarm navigation experiments at the German Aerospace Center (DLR).

C. Optimization problem

In KIS, the expected uncertainty of the state estimate $\hat{\boldsymbol{x}}^+$ gets minimized by moving the swarm along preferable trajectories. The uncertainty of the estimate is characterized by its mean square error (MSE)

$$\mathbb{\Sigma}_{\hat{\boldsymbol{x}}^+} = \mathbb{E}\left[\left(\boldsymbol{x}^+ - \hat{\boldsymbol{x}}^+ \right) \left(\boldsymbol{x}^+ - \hat{\boldsymbol{x}}^+ \right)^{\mathrm{T}} \right], \quad (7)$$

where $\mathbb{E}$ is the expected value over the probability density function $p\left(\boldsymbol{x}^+, \boldsymbol{z}^{(1:+)}\right)$, and $\boldsymbol{z}^{(1:+)}$ contains all collected measurements and predicted measurements for the next time step. We can take the weighted sum of the diagonal elements $\mathrm{tr}\left(\boldsymbol{\Lambda}_{\boldsymbol{x}^+} \mathbb{\Sigma}_{\hat{\boldsymbol{x}}^+}\right)$ as the cost function, with a diagonal weighting matrix $\boldsymbol{\Lambda}_{\boldsymbol{x}^+}$. The goal of information seeking is to choose admissible controls $\boldsymbol{u} \in \mathcal{V}$ such that the cost function is minimized, while fulfilling other mission objectives like collision avoidance, goal approaching, etc. The additional objectives are formulated as generic inequality constrains $\mathbf{g}(\boldsymbol{u}) \le \mathbf{0}$ as in [7]. The KIS optimization problem is then formulated as

$$\begin{aligned} \underset{\boldsymbol{u} \in \mathcal{V}}{\text{minimize}} \quad & \mathrm{tr}\left(\boldsymbol{\Lambda}_{\boldsymbol{x}^+} \mathbb{\Sigma}_{\hat{\boldsymbol{x}}^+}\right) \\ \text{subject to} \quad & \mathbf{g}(\boldsymbol{u}) \le \mathbf{0}. \end{aligned} \quad (8)$$

III. Kinematics-Aware Information Seeking

A. KIS formulated with PCRLB

The MSE of an estimator is lower bounded by the PCRLB [12], i.e.

$$\mathbb{\Sigma}_{\hat{\boldsymbol{x}}^+} \succeq \boldsymbol{\Sigma}_{\boldsymbol{x}^+} = \begin{bmatrix} \boldsymbol{\Sigma}_{\boldsymbol{p}^+} & \vdots \\ \cdots & \boldsymbol{\Sigma}_{\boldsymbol{\phi}^+} \end{bmatrix} = \boldsymbol{J}_{\boldsymbol{x}^+}^{-1}, \quad (9)$$

where $\boldsymbol{J}_{\boldsymbol{x}^+}$ is the Bayesian information matrix (BIM) expressed recursively in [13], $\boldsymbol{\Sigma}_{\boldsymbol{x}^+}, \boldsymbol{\Sigma}_{\boldsymbol{p}^+}$ and $\boldsymbol{\Sigma}_{\boldsymbol{p}^+}$ are the PCRLB of $\boldsymbol{x}^+, \boldsymbol{p}^+$, and $\boldsymbol{\phi}^+$, respectively, which are functions of the controls $\boldsymbol{u}$, and $\boldsymbol{A} \succeq \boldsymbol{B}$ denotes $\boldsymbol{A} - \boldsymbol{B}$ is positive semi-definite. If T is small enough, we can linearize (4) around

the expected state and the expected controls, i.e., $\bar{\boldsymbol{x}} = \mathbb{E}[\boldsymbol{x}]$ and $\bar{\boldsymbol{u}} = \mathbb{E}[\boldsymbol{u}]$, to further simplify the expression of the cost function to

$$\boldsymbol{x}^+ \approx f(\bar{\boldsymbol{x}}, \bar{\boldsymbol{u}}) + \frac{\partial \boldsymbol{x}^+}{\partial \boldsymbol{x}^{\mathrm{T}}}(\boldsymbol{x} - \bar{\boldsymbol{x}}) + \frac{\partial \boldsymbol{x}^+}{\partial \boldsymbol{u}^{\mathrm{T}}}(\boldsymbol{u} - \bar{\boldsymbol{u}}). \tag{10}$$

The BIM can then be written as

$$\begin{aligned}\boldsymbol{J}_{\boldsymbol{x}^+} &\approx \mathbb{E}_{\boldsymbol{x}^+}[\boldsymbol{I}_{\boldsymbol{x}^+}] + \left(\frac{\partial \boldsymbol{x}^+}{\partial \boldsymbol{x}^{\mathrm{T}}}\boldsymbol{J}_{\boldsymbol{x}}^{-1}\frac{\partial \boldsymbol{x}^{+\mathrm{T}}}{\partial \boldsymbol{x}} + \frac{\partial \boldsymbol{x}^+}{\partial \boldsymbol{u}^{\mathrm{T}}}\boldsymbol{\Sigma}_{\boldsymbol{u}}\frac{\partial \boldsymbol{x}^{+\mathrm{T}}}{\partial \boldsymbol{u}}\right)^{-1} \\ &= \begin{bmatrix}\mathbb{E}_{\boldsymbol{x}^+}[\boldsymbol{I}_{\boldsymbol{p}^+}] & \boldsymbol{0} \\ \boldsymbol{0} & \boldsymbol{0}\end{bmatrix} + \underbrace{\begin{bmatrix}\boldsymbol{\Sigma}_{\tilde{\boldsymbol{p}}^+} & \boldsymbol{\Sigma}_{\tilde{\boldsymbol{p}}^+,\tilde{\phi}^+} \\ \boldsymbol{\Sigma}_{\tilde{\boldsymbol{p}}^+,\tilde{\phi}^+}^{\mathrm{T}} & \boldsymbol{\Sigma}_{\tilde{\phi}^+}\end{bmatrix}^{-1}}_{\boldsymbol{\Sigma}_{\tilde{\boldsymbol{x}}^+}},\end{aligned} \tag{11}$$

where $\boldsymbol{\Sigma}_{\tilde{\boldsymbol{x}}^+}$ is the Cramér-Rao lower bound (CRLB) on the prediction of the next state $\boldsymbol{x}^+$ solely based on the transition model and previous estimation, $\boldsymbol{I}_{\boldsymbol{x}^+}$ and $\boldsymbol{I}_{\boldsymbol{p}+}$ are the predicted range-only FI in the next time step for the state and positions, $\boldsymbol{\Sigma}_{\tilde{\boldsymbol{p}}^+}$ is the CRLB of the predicted positions $\tilde{\boldsymbol{p}}^+$ without ranging, $\boldsymbol{\Sigma}_{\tilde{\phi}^+}$ is the CRLB of the predicted headings $\tilde{\phi}^+$ without ranging and $\boldsymbol{\Sigma}_{\tilde{\boldsymbol{p}}^+,\tilde{\phi}^+}$ is the coupling between the predicted positions and headings. Assuming that $p(\boldsymbol{x}, \boldsymbol{u})$ is unimodal and that position information from ranging changes slowly, we can approximate the expected value of the position information from ranging with its value at the expected position. After applying the Schur complement and the matrix inversion lemma several times, we obtain the final expression of PCRLB of the future positions and headings of agents as

$$\boldsymbol{\Sigma}_{\boldsymbol{p}^+} \approx \left(\boldsymbol{I}_{\boldsymbol{p}^+} + \boldsymbol{\Sigma}_{\tilde{\boldsymbol{p}}^+}^{-1}\right)^{-1} \tag{12}$$

$$\boldsymbol{\Sigma}_{\boldsymbol{\phi}^+} \approx \boldsymbol{\Sigma}_{\boldsymbol{\phi}} + T^2\mathbb{\Sigma}_{\dot{\boldsymbol{\omega}}} - \boldsymbol{\Sigma}_{\tilde{\boldsymbol{p}}^+,\tilde{\phi}^+}^{\mathrm{T}}\left(\boldsymbol{I}_{\boldsymbol{p}^+}^{-1} + \boldsymbol{\Sigma}_{\tilde{\boldsymbol{p}}^+}\right)^{-1}\boldsymbol{\Sigma}_{\tilde{\boldsymbol{p}}^+,\tilde{\phi}^+}.$$

The KIS problem in (8) can be approximated as

$$\begin{aligned}\underset{\boldsymbol{u}\in\mathcal{V}}{\text{minimize}} \quad & \mathrm{tr}\left(\boldsymbol{\Lambda}_{\boldsymbol{p}^+}\boldsymbol{\Sigma}_{\boldsymbol{p}^+}\right) + \mathrm{tr}\left(\boldsymbol{\Lambda}_{\boldsymbol{\phi}^+}\boldsymbol{\Sigma}_{\boldsymbol{\phi}^+}\right) \\ \text{subject to} \quad & \mathbf{g}(\boldsymbol{u}) \leq \boldsymbol{0},\end{aligned} \tag{13}$$

where $\boldsymbol{\Lambda}_{\boldsymbol{p}^+}$ and $\boldsymbol{\Lambda}_{\boldsymbol{\phi}^+}$ are diagonal weighting matrices of positions and headings, respectively. In (13) the original problem is explicitly expressed as two sub-problems, namely PIS and heading information seeking (HIS). This new formulation is preferable also because the cost function has a close-form expression w.r.t. the controls $\boldsymbol{u}$. In [7] the PIS is solved by signal-step gradient descent methods, which is not applicable for (13) due to the complex kinematic model. We apply the sequential least squares programming method proposed by [14], [15] to solve (13). This method iteratively searches for a quadratic approximation of a nonlinear objective function with inequality constraints.

B. KIS Solution Interpretation

We now investigate how the swarm behaves for KIS. For PIS, it has been shown in [7] that the swarm will move into the most rigid formation. In this paper, we focus on the HIS behavior. We assume the position and heading are approximately decoupled, and the range-only position information changes slowly. Consequently, we can consider each rover individually. The heading information gain can be approximated by

$$\begin{aligned}&\mathrm{tr}\left(\boldsymbol{\Lambda}_{\boldsymbol{\phi}^+}\boldsymbol{\Sigma}_{\tilde{\boldsymbol{p}}^+,\tilde{\phi}^+}^{\mathrm{T}}\left(\boldsymbol{I}_{\boldsymbol{p}^+}^{-1} + \boldsymbol{\Sigma}_{\tilde{\boldsymbol{p}}^+}\right)^{-1}\boldsymbol{\Sigma}_{\tilde{\boldsymbol{p}}^+,\tilde{\phi}^+}\right) \\ &\approx \sum_{i=1}^{N}[\boldsymbol{\Lambda}_{\boldsymbol{\phi}^+}]_{i,i}\left(\frac{\partial \boldsymbol{p}_i^+}{\partial \phi_i}\sigma_{\phi_i}^2 + \frac{\partial \boldsymbol{p}_i^+}{\partial \omega_i}\sigma_{\omega_i}^2 T\right)^{\mathrm{T}} \\ &\quad \times \left(\boldsymbol{I}_{\boldsymbol{p}_i^+}^{-1} + \boldsymbol{\Sigma}_{\tilde{\boldsymbol{p}}_i^+}\right)^{-1}\left(\frac{\partial \boldsymbol{p}_i^+}{\partial \phi_i}\sigma_{\phi_i}^2 + \frac{\partial \boldsymbol{p}_i^+}{\partial \omega_i}\sigma_{\omega_i}^2 T\right),\end{aligned} \tag{14}$$

where $\sigma_{\phi_i}^2$ and $\sigma_{\omega_i}^2$ are the PCRLB of the current heading and the variance of the turn rate, respectively. We observe that (14) is a quadratic form in a vector linearly combining $\partial \boldsymbol{p}_i^+/\partial \phi_i$ and $\partial \boldsymbol{p}_i^+/\partial \omega_i$, both of which are approximately perpendicular to the trajectory of the rover. Furthermore, the heading information gain is maximized if both vectors are aligned with the principal eigenvector of $(\boldsymbol{I}_{\boldsymbol{p}_i^+}^{-1} + \boldsymbol{\Sigma}_{\tilde{\boldsymbol{p}}_i^+})^{-1}$ corresponding to its largest eigenvalue. Especially when the range-only position information is small compared to the prediction, i.e., $\boldsymbol{I}_{\boldsymbol{p}_i^+} \ll \boldsymbol{\Sigma}_{\tilde{\boldsymbol{p}}_i^+}^{-1}$, the rover will move in trajectories that are perpendicular to the direction where the range-only position uncertainty is lowest. An example with three anchors is shown in Figure 3. The directions of the principal eigenvectors of $\boldsymbol{I}_{\boldsymbol{p}_i^+}$ (on the left) are pointing towards the anchors. The perpendicular lines to the principal eigenvectors are plotted on the right, forming multiple orbits around the anchors. The trajectories of two simulated agents applying HIS follow these orbits.

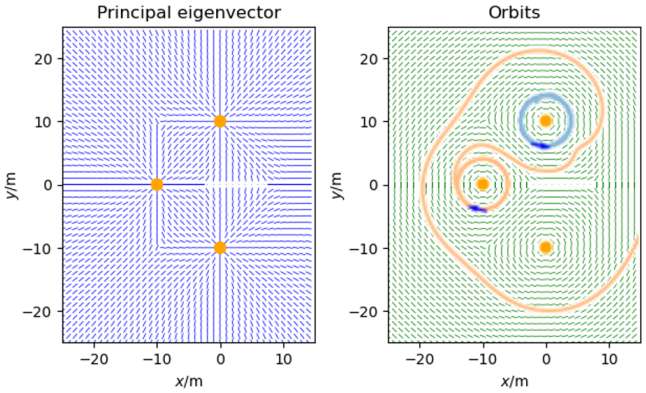

Figure 3: The directions of the principal eigenvectors (left) and the perpendicular lines to the principal eigenvectors together with trajectories of two agents applying HIS (right).

IV. Results

A. Large-Scale Swarm Simulation

To observe swarm behavior emerging from KIS at a large-scale, simulations with 20 rovers were performed (see Figure 4). A rover (the first one from the right) has to move to a goal $(x, y) = (100\,\mathrm{m}, 0\,\mathrm{m})$ with a minimal step of

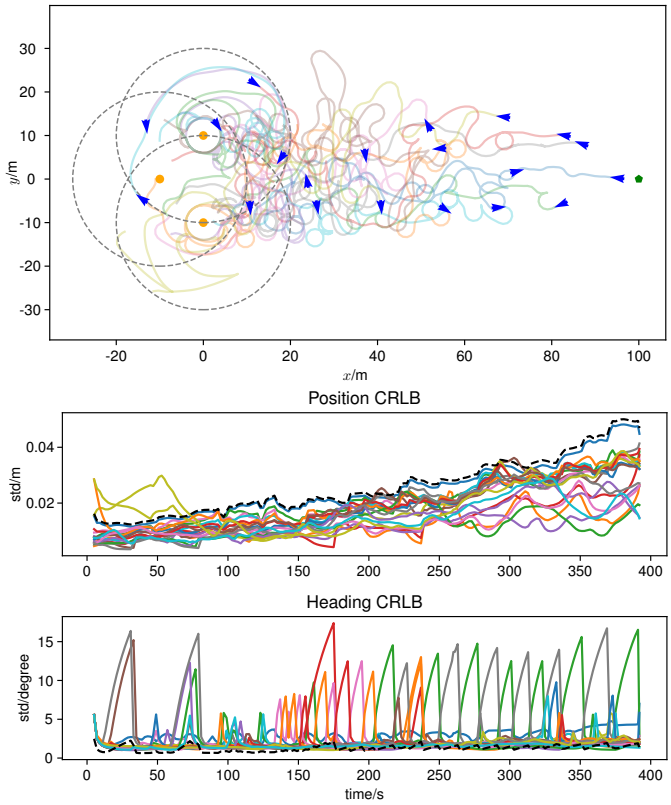

Figure 4: A 20-agent swarm applies KIS, while one agent (the first one from the right) additionally applies goal approaching.

$\delta_{\min} = 0.2\,\mathrm{m}$ per time step. The other 19 rovers support the goal-approaching rover by KIS. The maximum communication range is set to $20\,\mathrm{m}$ as in [16], which is visualized with gray dashed circles. Consequently, the goal-approaching rover cannot measure its distance to the anchors once it is outside the circles. It then relies on the other rovers to build a bridge back to the anchors for localization as seen in Figure 4 similar to the PIS behaviors presented in [7]. However, the agents of the bridge exhibit constant orbiting, wave-like and interweaving parallel movements, which results from the HIS component as expected in Section III-B. The square root of the position and heading PCRLBs are plotted in Figure 4. The spikes in the heading PCRLBs indicate that some agents are occasionally stationary to accumulate position information at a cost of increasing their heading uncertainty.

B. Space-Analogue Mission on Volcano Etna

As a highlight, the proposed KIS has been demonstrated in a space-analogue mission on the volcano Etna, Sicily, Italy, in July 2022. The experimental setup is shown in Figure 5. A lander and three sensor boxes are deployed at the landing site as anchors. Five agents including three stationary agents and two robots estimate their positions, velocities and orientations in 3D with real-time DPF [8]. The two rovers additionally apply KIS in real-time with their DPF output. The cost functions of KIS are extended to 3D, but the kinematics of

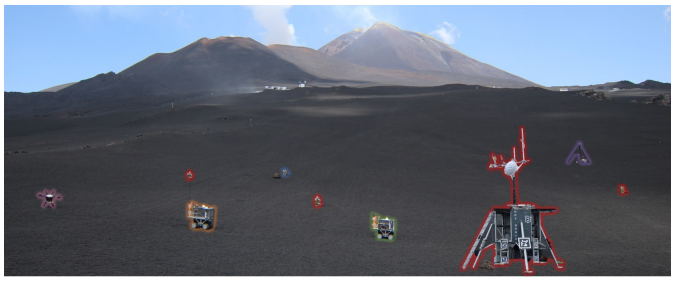

Figure 5: The experimental setup (viewed from the lander perspective) on the volcano Etna, Sicily, Italy, in July 2022.

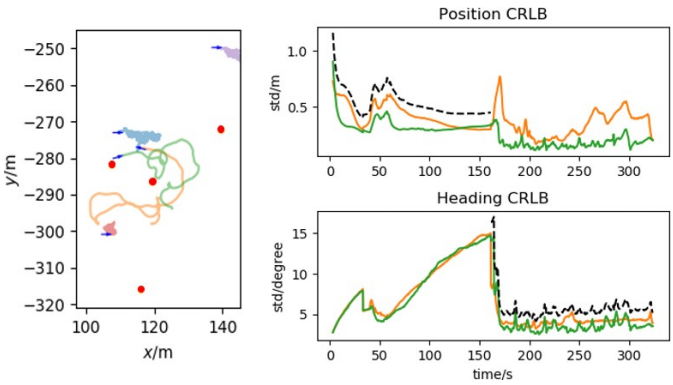

Figure 6: Estimated trajectories of all agents (left), positioning and orientation PCRLBs (right).

the rovers are constrained in 2D. The rovers firstly conduct PIS in the time interval of $30\,\mathrm{s}$ - $170\,\mathrm{s}$ and then switch to HIS at $170\,\mathrm{s}$. Some preliminary results of the experiment are plotted in Figure 6, including the estimated trajectories of all agents (left), positioning and orientation PCRLBs (right). The estimated trajectories of the agents qualitatively match well to the ground-truth trajectories recorded by real-time kinematic (RTK). Further quantitative analysis is still ongoing. As the outcome of PIS, rovers move to positions that are beneficial for position estimation of all agents, and then become stationary to accumulate position information. Meantime, the heading uncertainty increases. As soon as the rovers switch to HIS, they start moving around the anchors with orbiting behaviors, and the heading uncertainty drops.

V. Conclusion

We extended the swarm PIS framework in [7] to KIS. Agents in the swarm adapt their trajectories with given kinematic models to actively seek position and orientation information. A uncertainty measure based on PCRLB has been formally defined and exploited as cost functions. We analyzed the expression of PCRLB, which (a) helps us to find an efficient KIS solution, and (b) offers intuitive interpretation on the expected swarm behaviors. An orbiting behavior is predicted by theory and observed in both simulation and experiment. We demonstrated the real-time KIS swarm navigation in a space-analogue mission on the volcano Etna and pave our way to a real-world space swarm exploration mission.

REFERENCES

[1] L. Andreescu *et al.*, "100 radical innovation breakthroughs for the future," European Commission - Directorate-General for Research and Innovation, Tech. Rep. KI-01-19-886-EN-N, 12 2019. [Online]. Available: https://op.europa.eu/s/uxCF

[2] L. Abraham, S. Biju, F. Biju, J. Jose, R. Kalantri, and S. Rajguru, "Swarm robotics in disaster management," in *2019 International Conference on Innovative Sustainable Computational Technologies (CISCT)*, 2019, pp. 1–5.

[3] J. Liu, Z. Wang, Z. Peng, J.-H. Cui, and L. Fiondella, "Suave: Swarm underwater autonomous vehicle localization," in *IEEE INFOCOM 2014 - IEEE Conference on Computer Communications*, 2014, pp. 64–72.

[4] A. Wedler *et al.*, "From single autonomous robots toward cooperative robotic interactions for future planetary exploration missions," in *69th International Astronautical Congress (IAC)*, ser. Preceedings of the 69th International Astronautical Congress (IAC). International Astronautical Federation (IAF), 2018. [Online]. Available: https://elib.dlr.de/122782/

[5] S. Zhang, E. Staudinger, R. Pöhlmann, and A. Dammann, "Cooperative communication, localization, sensing and control for autonomous robotic networks," in *2021 IEEE International Conference on Autonomous Systems (ICAS)*, 2021, pp. 1–5.

[6] F. Meyer, H. Wymeersch, M. Fröhle, and F. Hlawatsch, "Distributed estimation with information-seeking control in agent networks," *IEEE Journal on Selected Areas in Communications*, vol. 33, no. 11, pp. 2439–2456, 2015.

[7] S. Zhang, R. Pöhlmann, T. Wiedemann, A. Dammann, H. Wymeersch, and P. A. Hoeher, "Self-aware swarm navigation in autonomous exploration missions," *Proceedings of the IEEE*, vol. 108, no. 7, pp. 1168–1195, 2020.

[8] S. Zhang, K. Cokona, R. Pöhlmann, E. Staudinger, T. Wiedemann, and A. Dammann, "Cooperative pose estimation in a robotic swarm: Framework, simulation and experimental results," in *2022 30th European Signal Processing Conference (EUSIPCO)*, 2022, pp. 987–991.

[9] S. Blackman and R. Popoli, *Design and Analysis of Modern Tracking Systems*, ser. Artech House Radar Library. Norwood, MA, USA: Artech House, 1999, p. 206.

[10] *Summit-XL datasheet*, Robotnik Automation S.L.L., 10 2021.

[11] E. Staudinger, S. Zhang, R. Pöhlmann, and A. Dammann, "The role of time in a robotic swarm: A joint view on communications, localization, and sensing," *IEEE Communications Magazine*, vol. 59, no. 2, pp. 98–104, 2021.

[12] H. L. Van Trees, *Detection, Estimation, and Modulation Theory*. John Wiley and Sons, Ltd, 2001, ch. 2, pp. 19–165. [Online]. Available: https://onlinelibrary.wiley.com/doi/abs/10.1002/0471221082.ch2

[13] P. Tichavsky, C. Muravchik, and A. Nehorai, "Posterior cramer-rao bounds for discrete-time nonlinear filtering," *IEEE Transactions on Signal Processing*, vol. 46, no. 5, pp. 1386–1396, 1998.

[14] D. Kraft, "A software package for sequential quadratic programming," *Forschungsbericht- Deutsche Forschungs- und Versuchsanstalt fur Luft- und Raumfahrt*, 1988.

[15] K. Schittkowski, "The nonlinear programming method of wilson, han, and powell with an augmented lagrangian type line search function," *Numerische Mathematik*, vol. 38, no. 1, pp. 83–114, 1982.

[16] S. Zhang, M. Frohle, H. Wymeersch, A. Dammann, and R. Raulefs, "Location-aware formation control in swarm navigation," in *2015 IEEE Globecom Workshops (GC Wkshps)*, 2015, pp. 1–6.